Engineering Structures 183 (2019) 124–134

Contents lists available at ScienceDirect

Engineering Structures

journal homepage: www.elsevier.com/locate/engstruct

Repair assessment for distortion-induced fatigue cracks in a seismically retrofitted double-deck bridge complex

Mehdi Motaleb[a], Will Lindquist[b,*], Ahmed Ibrahim[c], Riyadh Hindi[a]

[a] Parks College of Aviation, Engineering and Technology, Saint Louis University, St. Louis, MO 63103, United States
[b] William Jewell College, Liberty, MO 64068, United States
[c] College of Engineering, Department of Civil and Environmental Engineering, University of Idaho, Moscow, ID 83843, United States

ARTICLE INFO

Keywords:
Distortion-induced fatigue
Web-gap cracking
Seismic retrofit
Damage
Field test
Load testing

ABSTRACT

Many steel bridges in the United States designed before the mid-1980s are highly susceptible to distortion-induced fatigue cracking. This vulnerability is substantially increased if the out-of-plane driving force caused by differential girder displacement is increased for any reason. This research examines one such case where a double-deck bridge complex, originally built in the 1960s, was retrofitted to improve seismic performance. As part of the retrofit, single angle K-type diaphragms were replaced with stiffer double-angle cross-type diaphragms. This seismic retrofit led to an increase in web-gap stresses, and within approximately one year following the retrofit, inspectors identified numerous fatigue cracks in the web of longitudinal girders where connection plates terminate near top flanges. A repair measure was implemented to provide a positive connection between the connection plate and the girder flange. The purpose was to reduce the high stress concentrations in the web-gap region by restricting the out-of-plane distortion in the web-gap region. Field tests were carried out in addition to developing finite element (FE) models to investigate the efficacy of the repair technique. The results confirmed a significant decrease in the web-gap stress after implementation of the repair, and a subsequent FE analysis showed that the new load path through the repair angle section did not introduce a new fatigue sensitive area. In fact, the repair resulted in stresses well below the constant amplitude fatigue threshold (CAFT) for this type of detail.

1. Introduction

Most continuous-span double-deck viaducts built in the San Francisco Bay Area during the 1950s and 1960s were damaged during the 1989 Loma Prieta earthquake [1]. The deficiencies in these viaducts led to an immediate review of all double-deck bridge structures in the United States. One particular seismic retrofit project (and the focus of this work) involved a Midwestern double-deck bridge complex with substructure and superstructure elements without adequate capacity based on current seismic criteria [2,3]. A seismic retrofit strategy was adopted based on the criteria described in the FHWA Seismic Retrofitting Manual for Highway Bridges [4]. Almost immediately following completion of the seismic retrofit, horseshoe-shaped cracks were identified in the unstiffened regions (frequently called the web gap) of the longitudinal girders where the original K-type diaphragms were replaced with new, stiffer cross-diaphragms. This problem mostly occurs in bridges built in the United States prior to the mid-1980s when the design specifications required connection plates to have a tight-fit detail at the girder flanges, but not welded [5–7].

Normally, part of the connection plate, attached to plate girders, must be clipped to clear the web-to-flange weld resulting in a soft and short section that is more flexible in the transverse direction than the rest of the girder's height. This area in the web is known as the web-gap region. Cracks originating in this region are likely the result of secondary stresses resulting from out-of-plane distortion in the unstiffened web-gap region and account for approximately 90% of all fatigue cracking [23]. As a result, a significant number of older bridges have been affected by distortion-induced fatigue cracking in the web-gap region.

Several previous studies have focused on fatigue crack initiation and damage assessment of steel bridge details using fracture mechanics approaches, numerical simulations, laboratory testing, and bridge instrumentations [8–13]. Meanwhile, finding solutions to mitigate cracking continues to be of interest to researchers. Several experimental projects have been conducted to identify potential repair methods for distortion-induced cracking in the web-gap regions of steel girder

* Corresponding author.
E-mail addresses: lindquistw@william.jewell.edu (W. Lindquist), aibrahim@uidaho.edu (A. Ibrahim).

https://doi.org/10.1016/j.engstruct.2019.01.004
Received 10 March 2017; Received in revised form 5 September 2018; Accepted 1 January 2019

bridges [14–18]. Most of the repair methods can be categorized as either web-gap stiffening or web-gap softening strategies which are summarized by Dexter and Ocel [16]. Repair techniques which are not directly aimed at stiffening or softening the web-gap include hole drilling, diaphragm removal, diaphragm repositioning, and bolt loosening [16,19–22].

Connor and Fisher [23] conducted field instrumentation, testing, and long-term remote monitoring to assess the effectiveness of existing retrofits introduced at the stiffener ends and at gusset plates for a three-span continuous haunched plate-girder bridge. Their test results showed that two small 3 × 3 × 3/8 angles attached with two bolts were not capable of providing enough rigidity between the gusset and transverse connection plate in order to keep the web-gap stresses below the constant amplitude fatigue limit for a Category C detail. However, their study demonstrated that retrofits with heavier 8 × 8 × 5/8 angles attached to the transverse connection plate and girder flange with more bolts were effective at reducing the out-of-plane distortion and cyclic stresses. They reported that evaluation of stress ranges is often needed from field measurements in order to accurately model and understand the complex behavior resulting in fatigue damage [23].

Shifferaw and Fanous [24] examined the behavior of web-gap distortion of a skewed multi-girder steel bridge through field testing and finite element (FE) studies. The field portion of the research was conducted on a bridge with an existing retrofit for a non-cracked web-gap. They evaluated the effectiveness of various retrofit methods and concluded that simply loosening the bolts between the existing connection plate between the stiffener and the girder top flange was effective in reducing induced stresses in the web-gap region.

Previous studies [25,26] conducted on bridges similar to the one being investigated in this paper identified the cause of cracking through FE analysis and field instrumentation. These studies also recommended several preliminary repair options. This work deals with the bridge after implementing pilot repairs to evaluate their effectiveness by comparing the data from both field tests and FE analyses. Measurements taken from the test (after the repair) were compared with those measurements taken from the first field test (before the repair) to determine the stress reduction in the web-gap region resulting from the repair. Finite element models were developed as part of this work to estimate stresses in the upper web-gap regions and enable investigation of the crack propagation potential in the web-gap region.

2. Bridge description

The bridge described in this paper represents one section from a larger double-deck bridge complex approximately 2.41 km (1.5 miles) in length that carries more than 93,000 vehicles per day and designed in the 1960s [27].

2.1. Superstructure description (original bridge)

The bridge is comprised of a composite reinforced concrete deck with a multi-steel plate girder superstructure supported by transversal steel box beams seated on reinforced concrete columns. The section under consideration is from the upper deck and between expansion joints and consists of four spans each with a length of approximately 21.4 m (70.2 ft.).

A plan view of the original bridge, prior to implementation of the Department of Transportation DOT) mandated seismic retrofit, is shown in Fig. 1(a) with cross girders labeled according to their number relative to the entire complex. The K-type intermediate diaphragms consist of L3-1/2 × 3–1/2 × 5/16 angles for the top chords and L3 × 2–1/2 × 5/16 angles for the remaining members, as shown in Fig. 1(b).

2.2. Seismic retrofit description

The seismic retrofit strategy was necessary to resist horizontal shear forces (both in the longitudinal and transverse directions) which were not accounted for in the original design [2,28]. Structural modifications were made to the upper superstructure and supporting columns to resist horizontal shear in both the longitudinal and transverse direction as well as displacements in both directions. Concrete columns were retrofitted to improve the performance in the transverse direction, and a framework of rolled W12 sections connected to the existing exterior girders and the concrete columns was used to provide additional resistance against shear in the longitudinal direction. This framework (cross girder retrofit) were connected to the exterior girders at the nearest diaphragm, as shown in Fig. 2. The structural modification resulted in increasing the load demand at these locations and a stiffer diaphragm system was necessary. Hence, the existing K-diaphragms were replaced by cross-diaphragms consisting of 2L4 × 4 × ⅜ double angles, also shown in Fig. 2.

2.3. Web-gap cracking

Within approximately one year following the completion of the seismic retrofit, the DOT inspectors identified several cracks in the webs of the longitudinal plate girders during a routine inspection. The cracks were a combination of horizontal cracks formed at the web to upper flange joint and horseshoe-shaped cracks originating from the stiffener-to-web intersection, as shown in Fig. 3. These cracks were predominately located in the three interior girders at the location of the cross-girder retrofit and new cross-diaphragms, as shown in Fig. 2.

2.4. Pilot repair measure

A repair solution was developed for the cracked region based on findings from previous analytical studies [25,26]. The repair strategy ultimately selected was to positively attach the connection plate (stiffener) to the upper flange [25] with WT 12 × 88 × 5 sections with the flange removed on one side, as shown in Fig. 4. Nelson HBL Full Base 3/4 × 2–3/4 thread studs were used to connect the angle section to the top flange and 3/4-in. diameter bolts were used to tighten the two angle flanges and the connection plate together.

3. Bridge instrumentation

Two field tests were performed in order to estimate the actual stress conditions in the field. The first field test was conducted on the seismically-retrofitted structure prior to the web-gap repair, and the second field test was conducted after a pilot top-angle repair was completed, as shown in Fig. 4. The field test involved strain gage instrumentation at three general locations (web-gap region, bottom flange, and cross-diaphragm leg) including a total of 22 unidirectional strain gages. All strain gages with nominal resistances of 350 O were connected to a CR3000 data logger using three-wire quarter bridge connections. The three-wire strain gage minimizes temperature-induced resistance changes in the leads, as well as reduces the sensitivity effect that the wires have on the gage [29].

A preliminary FE model using SAP2000, described in [26], was used to guide the strain gage arrangement for the field tests.

3.1. Locations of interest and layout of instruments

3.1.1. Web-Gap

The north side of girder 2 (G2) and the south side of girder 4 (G4) at station 11 were selected to attach the strain gages in the web-gap region, as shown in Fig. 5. At each location, three strain gages were placed over 25.4-mm (1-in.), the top gage being positioned 19.1 mm (0.75 in.) from the bottom of the top girder flange, and 30.5 mm (1.2

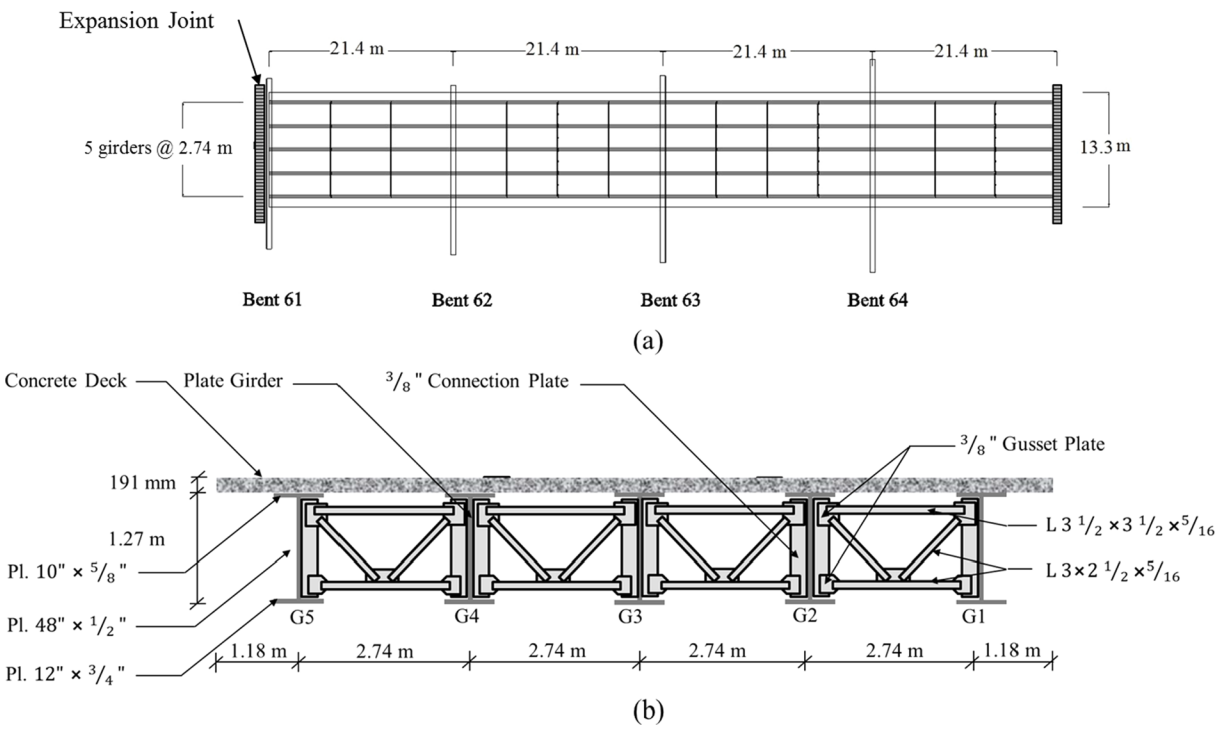

Fig. 1. Original bridge (a) plan-view and (b) cross-view.

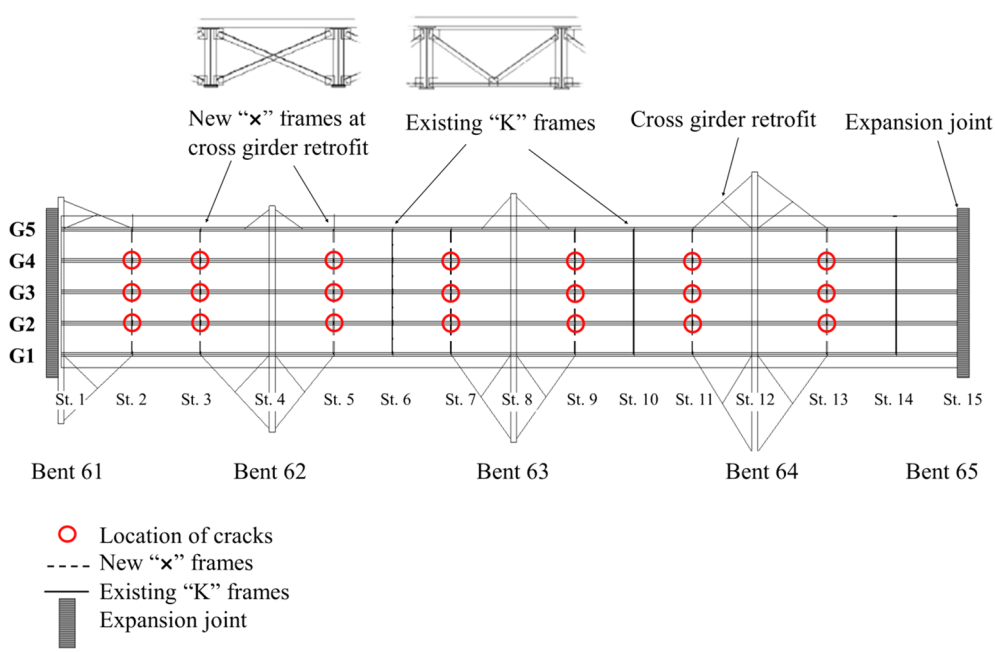

Fig. 2. Seismic retrofitted bridge plan-view.

in.) from the connection plate surface. Fig. 6 shows the layout and detailed arrangement of these gages in the web-gap region for the first and second field tests. The vertical location of the gages shifted downward for 25.4 mm (1 in.) placing them 44.5 mm (1.75 in.) from the bottom of the top flange for the second trial. This relocation was necessary as the repair angle was in the original location of the gages in the first field test.

3.1.2. Bottom flange of longitudinal girders and cross girder

Unidirectional strain gages were attached under the middle of the bottom flange and spaced 50.8 mm (2 in.) away from each other, as shown in Fig. 7. The gages were attached under the tension flange of longitudinal girders 2 and 4 at station 11 and longitudinal girders 2 and 3 at station 10, as shown in Fig. 5. Also, two unidirectional strain gages were attached under the bottom surface of the cross girder at bent 64 (station 12). These measurements were used for comparisons to numerical models as the stress distribution is less complicated away from stress concentrations.

3.1.3. Cross-bracing diaphragms

Three strain gages were attached in two different locations on the legs of the cross-diaphragm connecting girders 2 and 3 and girders 3 and 4. They were placed at a distance of 635 mm (25 in.) from the end of the cross-diaphragm connected to the stiffener, as shown in Fig. 5.

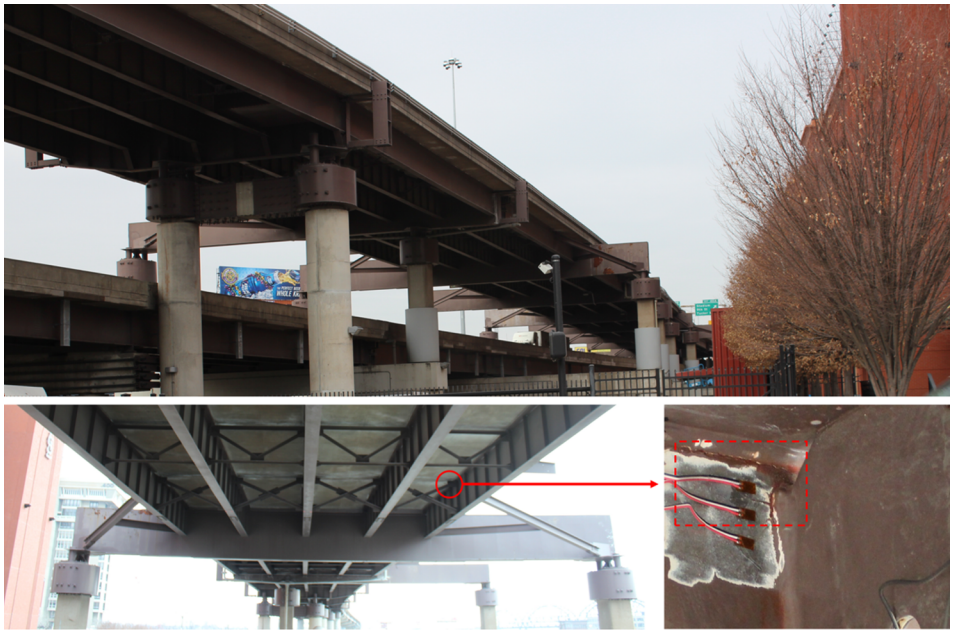

Fig. 3. Double-deck bridge complex and the location of horseshoe cracks and horizontal cracks.

Fig. 4. Repaired web-gap view.

The layout of the instrumentation on the cross-diaphragm is shown in Fig. Fig. 8.

4. Test procedure

For the first field test, a loaded rear tandem axle DOT truck with a gross weight of 25.4 tons (55.9 kips) was used to load the bridge. Three load cases were used corresponding to placement of the truck in each of the three driving lanes (right lane, middle lane, and left lane) at the left of bent 64 while the back tandem was located on cross girder (station 12). This location in longitudinal direction was used for consistency between all load case and was close to the critical truck location identified in the FE analysis resulting in maximum web-gap stress when an HS-20 truck loading was applied to the bridge [26]. During the test, the truck stopped at each of these predefined locations for approximately 10 min.

A similar loading procedure was used for the second field test

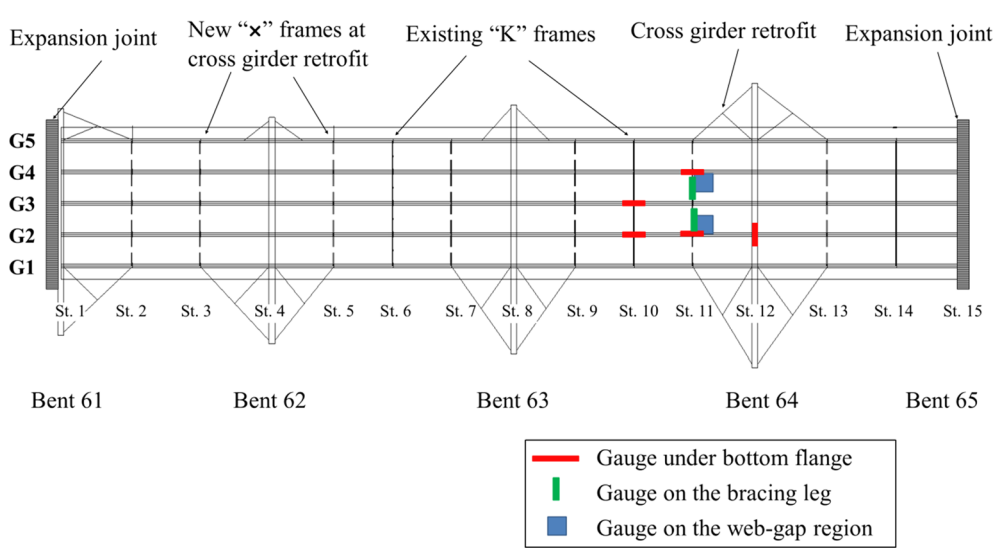

Fig. 5. Plan view illustrating strain gage locations.

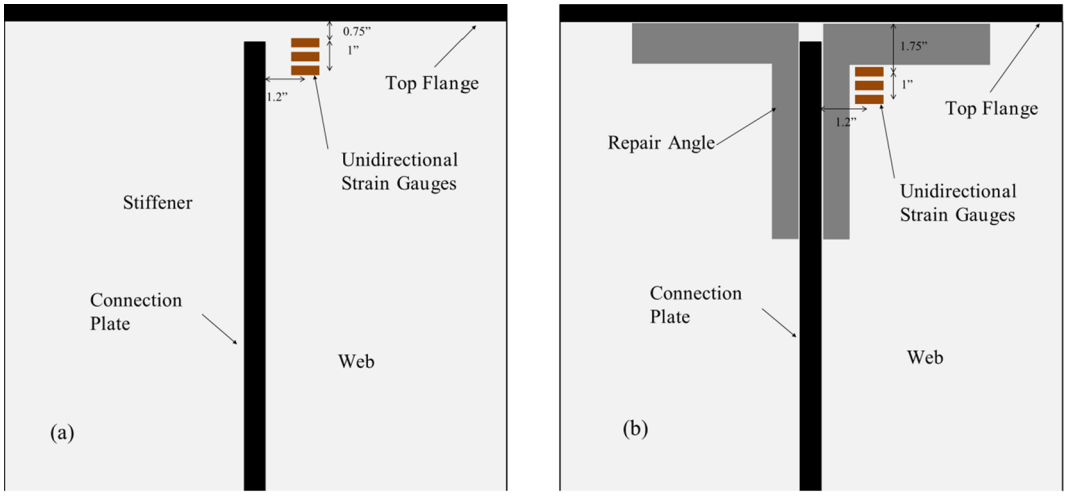

Fig. 6. Web-Gap strain gage arrangement for the (a) first field test, and (b) second field test.

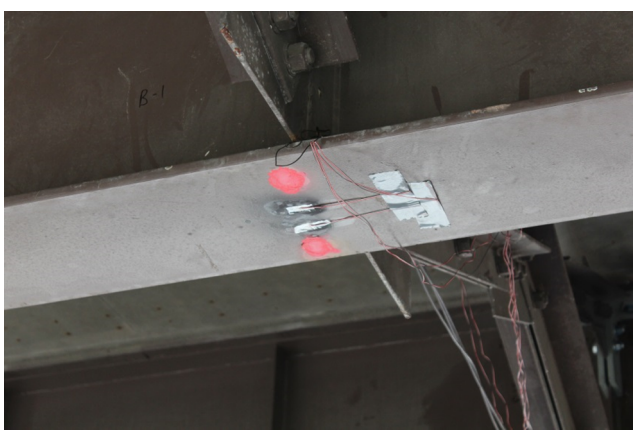

Fig. 7. Position of strain gages under the bottom flange.

following the pilot repair. However, the loaded truck gross weight was 26.9 tons (59.2 kips) which was slightly heavier than the first truck. A picture of the truck and the axle load distribution is shown in Fig. 9.

5. Field test results

The first field test was conducted to verify the existence of high stresses in the cracked web-gap region of the interior girders, and the second field test was performed to evaluate the effectiveness of the pilot repair measure. Table 1 summarizes the corresponding stresses (calculated using Hooke's law) for both field load tests. The web-gap stress for G2 and G4 are reported as top, middle, and bottom referring to the position of the strain gages in the web-gap. The average gage reading is reported for locations with multiple strain gages.

The first field test data indicates that the highest web-gap stress of 88.3 MPa (12.8 ksi) occurred in G2, with the truck positioned in the middle lane. This stress was captured from the gage positioned on the top level of the 3-gage group. The middle lane was the critical load case for web-gap stress in G4 as well. The web-gap stress ranges between 30 MPa (4.35 ksi) and 43 MPa (6.24 ksi) for this girder.

A second field test was performed following completion of the pilot repair. The majority of strain gages were attached in the same location as the first field test. However, the angle repair in the web-gap region of the girders resulted in limited space for the strain gages, and as a result, the location of the three-gage set in the web-gap region was moved down 25.4 mm (1 in.). This relocation was necessary due to the lack of access after adding the repair angle sections. The exact location of the

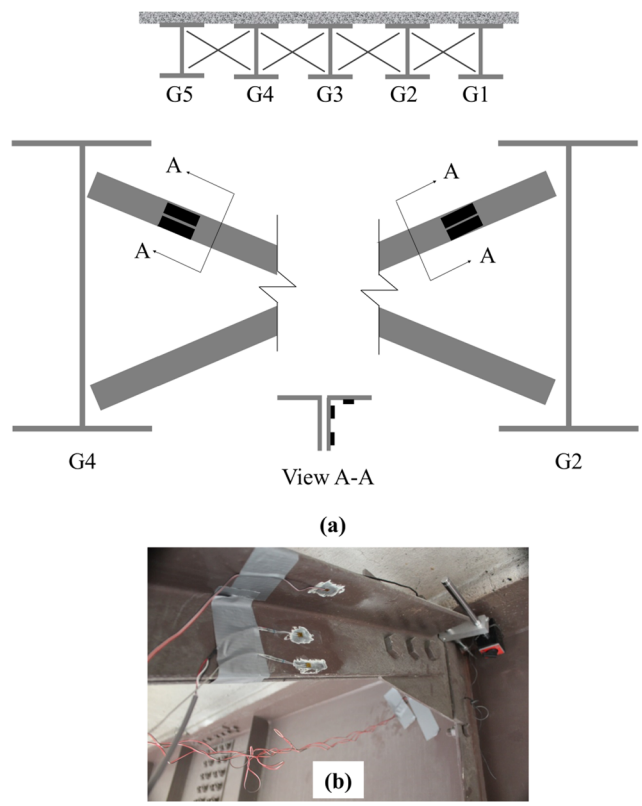

Fig. 8. ×-diaphragm instrumentation, (a) strain gage arrangement, (b) instrumented bracing view.

gages in the web-gap region is shown in Fig. 6. Also, for an unknown reason, one of the gages in the web-gap region of G2 malfunctioned and is not reported herein.

The highest measured stress in the web-gap region was 10.7 MPa (1.55 ksi) for the gage positioned on the top level of the 3-gage group in G4, as reported in Table 1, with the truck positioned in the middle lane. Girder 2 also experienced the maximum web-gap stress when the truck load was applied in the middle lane with stresses that varied between 1.29 MPa (0.187 ksi) and 4.85 MPa (0.703 ksi). Similar to the first field test, the results validated that loading the middle lane resulted in the highest web-gap stresses in the interior girders. Loading the left lane produced the second highest stress for G4 and loading the right lane resulted in the second highest stress value in the web-gap region of G2.

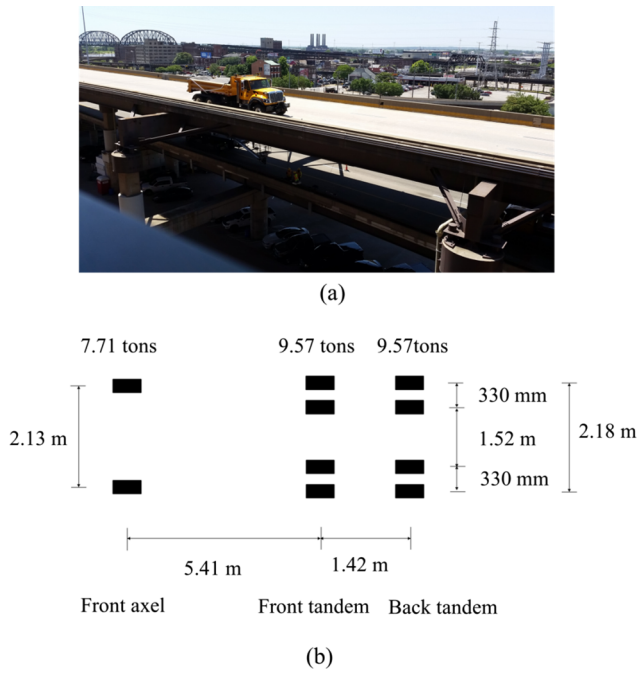

Fig. 9. Second field test with the (a) truck in the right lane, and (b) truck axle load distribution.

The equivalent average stresses in the longitudinal girder and cross girder were below 10.8 MPa (1.57 ksi) which is slightly greater than 8.76 MPa (1.27 ksi) measured during the first field test which can be attributed to the difference in truck weights.

5.1. Comparison between first field test and second field test

The bottom gage in the three-gage set in the web-gap region of interior girders in the first field test was positioned at the same location as the gage positioned at the top of the three-gage set in the second field test, as shown in Fig. 6. Hence, these two individual gages were used to conduct a comparison between stresses at the same location before and after the repair. Also, the average of the three-gage readings in the web-gap was used as another comparison between the first and second field tests. The field test data indicates a significant reduction in stress for the gages attached in the web-gap region.

As Figs. 10 and 11 show, there is a considerable decrease in the web-gap stress of G2 and G4 after repairing the bridge. The web-gap stress reduction in G2 for the three load cases are 90%, 129%, and 61% when the truck load is applied to the middle, right, and left lane, respectively.

Also, the readings from the single gage with the same location for both field tests showed a significant reduction in the web-gap stress for G4 with reductions of 75%, 94%, and 83% when the truck load was applied to the middle lane, right lane, and left lane, respectively. It is clear based on this comparison that the repair was effective in reducing stresses.

Figs. 12 and 13 show a comparison of average stresses for the three gages attached in the web-gap region of G2 and G4 after completion of

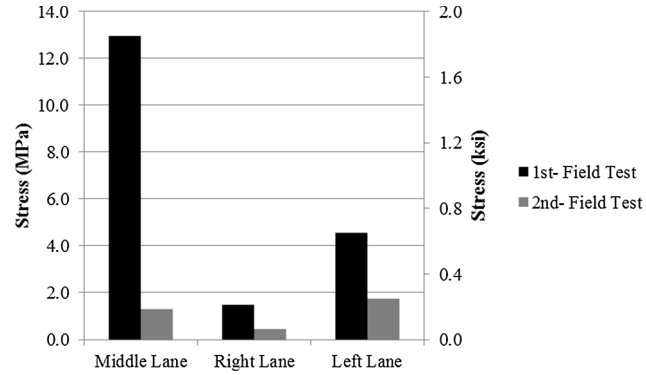

Fig. 10. Comparison between stress of a single gage in the web-gap of G2 before and after repair.

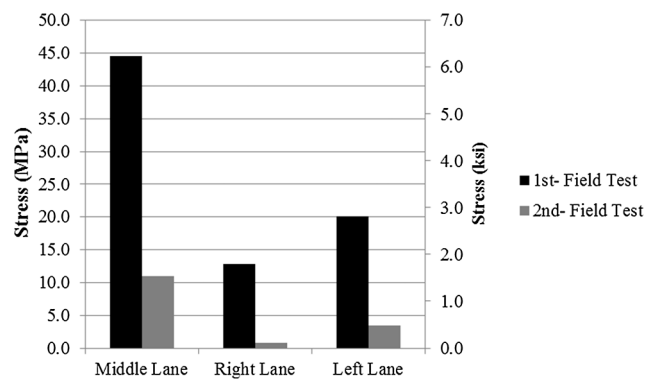

Fig. 11. Comparison between stress of a single gage at web-gap of G4 before and after repair.

Table 1
Field test results.

Gage position		1st-Field test stresses Truck location			2nd-Field test stresses Truck location		
		Middle (MPa)	Right (MPa)	Left (MPa)	Middle (MPa)	Right (MPa)	Left (MPa)
Web-gap G2	Top	88.3	33.6	−1.86	1.29	0.434	1.76
	Middle	9.94	−6.72	4.10	N/A*	N/A*	N/A*
	Bottom	13.0	−1.48	4.54	4.84	1.16	1.84
Web-gap G4	Top	39.0	8.94	14.7	10.7	0.758	3.28
	Middle	30.0	9.40	15.0	9.86	0.798	3.29
	Bottom	43.0	12.4	19.4	8.42	0.762	2.56
x-Diaphragm G2-G3	Average	2.00	0.46	0.232	13.4	2.41	2.77
x-Diaphragm G3-G4	Average	2.32	−0.036	0.228	11.0	2.17	2.18
G2 st.10	Average	3.24	1.41	2.14	3.23	2.06	2.63
G2 st. 11	Average	6.42	1.11	6.70	5.51	2.25	7.53
G3 st.10	Average	3.04	2.70	1.83	2.88	2.88	2.43
G4 st. 11	Average	5.64	4.96	−0.212	4.36	3.68	2.54
Cross girder	Average	7.24	4.54	8.76	7.59	5.59	10.8

* The strain gage malfunctioned and is not reported.

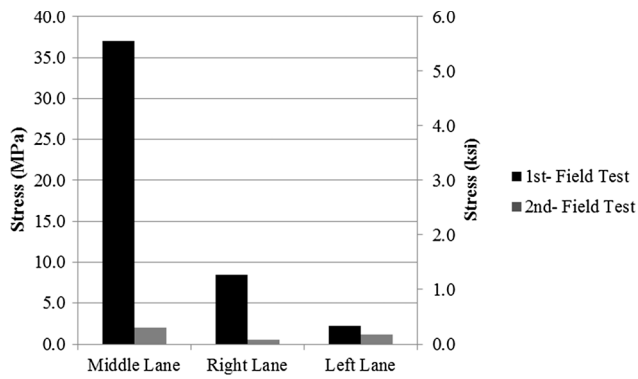

Fig. 12. Comparison between average stresses of three gages at the web-gap of G2 before and after repair.

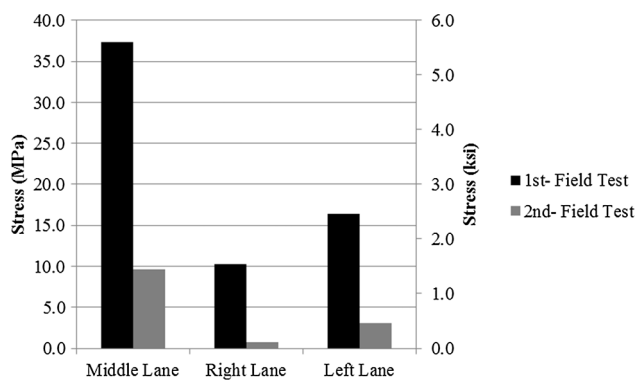

Fig. 13. Comparison between average stresses of three gages at the G4 web-gap before and after the repair.

the pilot bridge repair. The average stress in G2 is reduced by 92% following the repair with the middle lane loaded. This reduction is 91% and 21% when the truck is located in the right and left lane, respectively. Average stresses measured by the three gages at the G4 web-gap are reduced by 74% when the truck load is applied to the middle lane, 93% when truck load is applied to the right lane, and 81% when the truck load is applied to the left lane.

6. Finite element analysis

A comprehensive 3-D finite element analysis (FEA) including a macro-model and a micro-model was performed for the four-span section using Abaqus/CAE. The objective was to estimate the stresses in the upper web-gap regions to investigate the crack propagation potential for the repaired bridge due to live loads. Fig. 14 shows the macro-model that included a four-span portion of the bridge between expansions joints, and Fig. 15 shows the micro-model that consisted of a 5.08 m (200 in.) section including the transverse diaphragm at station 11 and the critical web-gap region in G2 [25]. All boundary conditions (displacement and rotation) for the micro-model were imported from the macro-model. The loads were applied as static loads to simulate the loads applied during the field tests which were stationary.

Tie interactions were used to model the composite action between the concrete deck and longitudinal girders. Also, all the connections between structural members located away from the location of interest were considered fully bonded. Surface contact interactions were defined for each bolt and the surrounding members with hard normal contact and friction coefficient of 0.5. The pre-tensioning forces in the bolts were applied to the middle of the shank in the first step of the analysis so that each carried a specified pretension force of 227 kN (51 kips) as defined by AASHTO [32] for 25.4-mm (1-in.) diameter bolts. The welds were idealized using right triangles and modeled using eight-node solid elements tied on each side to the base metal. Finite element models were created using 3D solid eight-node elements with three translational degrees of freedom and reduced integration (C3D8R). The reduced integration elements use lower-order integration to form the element stiffness while the mass matrix and distributed loadings use full integration. These elements reduce run time, especially in three dimensions [30].

Mesh density optimization was performed using various element sizes for G2, which includes the web-gap under investigation in this research. An element size of 5.08 mm (0.2 in.) was selected for G2 as the hotspot stresses in the web-gap region converged to a constant value. A coarser mesh of 120 mm (4.75 in.) was used for the other girders away from the location of interest. The models contained approximately one million elements. All simulations were run on a node of Saint Louis University's cluster including 20 CPUs and 250 GB RAM and required an average total CPU time of approximately 15,000 s for running each micro-model simulation.

The localized stress distribution in the web-gap region showed that cracks originated from the stiffener-to-web intersection (horseshoe-shaped cracks) and formed on the side of the web that experiences tension from the diaphragm. The other group of cracks at the web-to-upper flange joint (horizontal cracks) formed on the opposite side of the web. Thus, two set of stresses are compared to evaluate the effectiveness of the repair in reducing these stresses causing crack development. The hot-spot stress method was used to compare the localized stress in the web-gap region and maximum principal stress along the horizontal fillet weld of the web-to-flange joint on the opposite side of the web surface for various models. The hot spot stresses were calculated by extrapolating stress values at distances of 0.5 t and 1.5 t, where "t" is web thickness, measured perpendicular from the weld toe to estimate the stress at the weld toe (additional details are provided in [25]). It is important to note that the stresses shown prior to the repair do not include the softening effects expected as a result of cracking.

6.1. Verification of finite element modeling

In order to verify the simulation of the bridge, results from the FE model were compared with the corresponding field test results of the bridge before the repair (first field test measurements). The results from the FE analysis are compared with results from field measurements for stresses at the bottom flange of G2 and G4, as shown in Fig. 16. As this figure shows, the FE and field test results were consistent in determining the location of maximum stress in the longitudinal girders for each load case. However, the bending stresses in the longitudinal girder obtained from the FE showed higher values than those measured in the field test. Fig. 17 compares the bending stresses at cross girder for all three load cases. The FE results and field test measurements identify the same trend in stresses (location of minimum and maximum stresses) even though there is a difference between stress values. The reason for these differences could be attributed to a number of factors. First, all the originally designed stiffeners inside the cross girder were modeled but it is plausible that some of them might not be fully functional as they are hidden inside the box girder. Second, all material properties were assumed perfect in the FE model while the material properties in the bridge that has been in service since 1964 could change due to aging and corrosion.

6.2. Stress distribution in the web-gap region

The bridge following the repair was simulated by modifying the verified FE model of the bridge prior to the repair. Fig. 18 shows the FE models with views of the instrumented web-gap region of G2 before and after the repair. For consistency purposes, a similar truck was used for loading both models.

Among the three load cases, the field test results for the truck in the middle lane were considered for investigating the stress distribution in

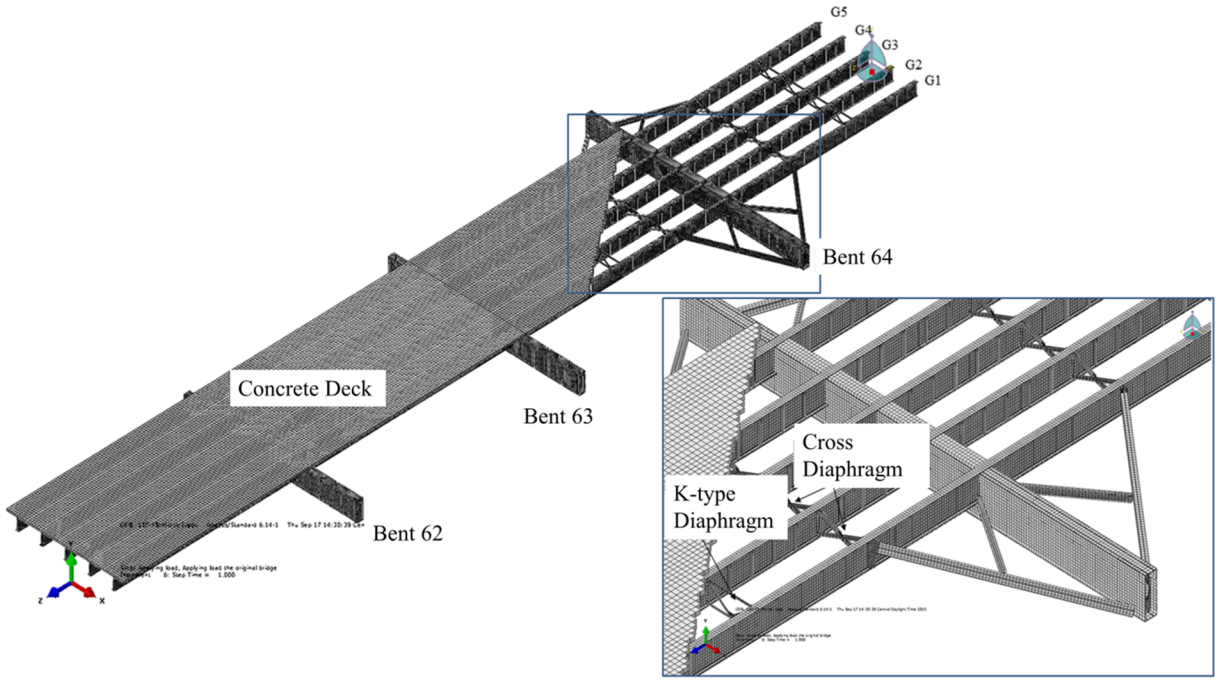

Fig. 14. Macro-model created using Abaqus/CAE.

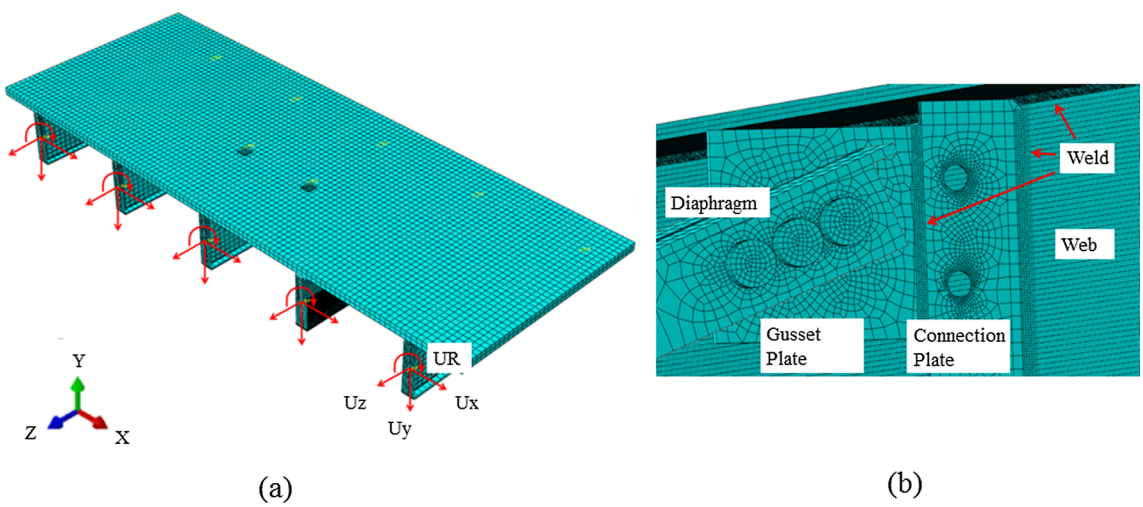

Fig. 15. (a) Micro-model created using Abaqus/CAE (b) Detailed connection in the web-gap region.

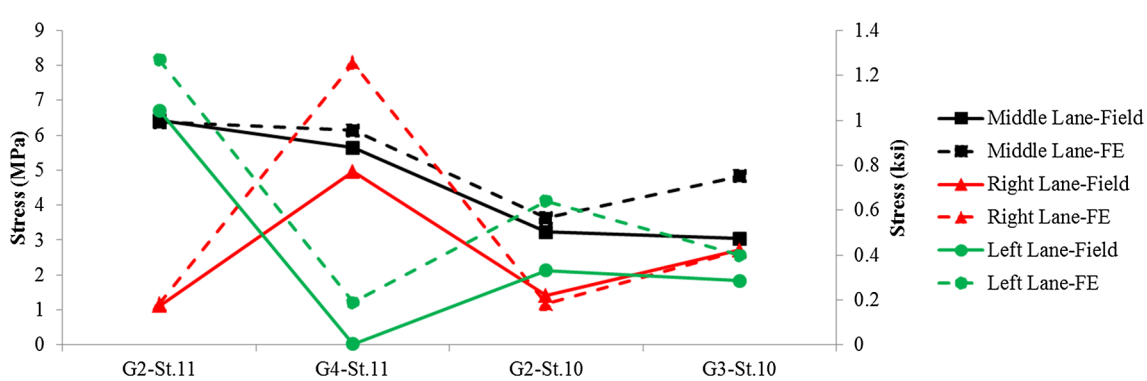

Fig. 16. Stress comparison between first field tests and FE for longitudinal girders.

the web-gap region obtained from the FEA. This represented the critical loading condition which resulted in the maximum differential deflection between adjacent girders and the maximum web-gap distortion at G2. Fig. 19 illustrates the stress distribution in the web-gap region of G2 before and after the repair. The localized maximum principal stresses after the repair occurred at the same location as before the repair and

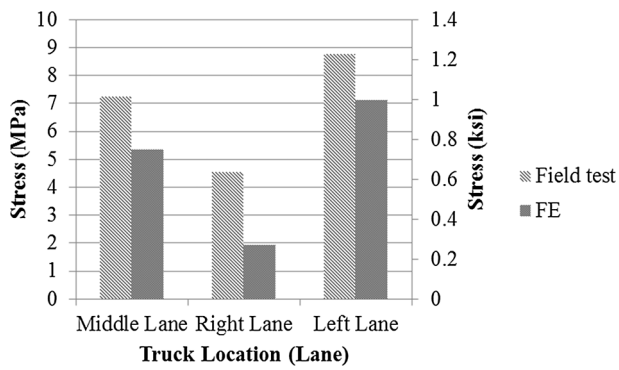

Fig. 17. Stress comparison between first field tests and FE for cross girder.

they are smaller in magnitude and act over a much smaller area. These results demonstrate that the new load path through the repair angle section did not introduce a new critical fatigue sensitive area.

Fig. 20 shows the hot-spot stress for the web-gap of G2 prior to the seismic retrofit for the original bridge, after the seismic retrofit (before web-gap repair), and after the web-gap repair. The hot-spot stress is reduced by 62% from 103 MPa (14.9 ksi) to 39.0 MPa (5.65 ksi) which is slightly higher than the stress calculated for the original bridge.

Fig. 21 shows the maximum principal stress along the horizontal fillet weld of the web-to-flange joint on the web surface for G2 when the middle lane of the bridge is loaded. As Fig. 21 shows, the peak stress along the web-to-flange joint drops dramatically from 125 MPa (18.1 ksi) to 38.6 MPa (5.60 ksi) when the repair strategy is implemented.

For the unrepaired bridge, the results indicate that the hot-spot stress and the peak stress along the horizontal fillet weld of the web-to-flange both exceed the constant amplitude fatigue threshold (CAFT) of 68 MPa (10 ksi) [31,32]. Consequently, distortion-induced fatigue cracks associated with the web-gap stress and the web-to-flange joint stress can occur after only a limited number of cycles. Also, the comparison between the results before and after the repair indicate that the web stresses are well below the CAFT and it is therefore expected to not experience new distortion-induced fatigue cracking.

7. Summary and conclusions

Distortion-induced fatigue cracking was identified during an annual inspection in the web-gap region of interior girders of upper level deck in a double deck bridge. Field measurements and FEA provided extensive data to investigate the cause of cracking and the effectiveness of the repair by comparing the web-gap stresses before and after implementing a repair strategy (providing a positive connection between the stiffener and the top flange of the girder). The performance of the bridge in the FE model was verified against field test measurements. The FE model was used to investigate the distribution of stresses in the web-gap region after the repair. Field measurements indicate the following:

- Loading the bridge in the middle lane was found to create the highest stresses in the web-gap region of G2 and G4 which is consistent with results from the FE study.
- The field test results conducted after the pilot repair showed a considerable reduction in the web-gap stress of the interior girders

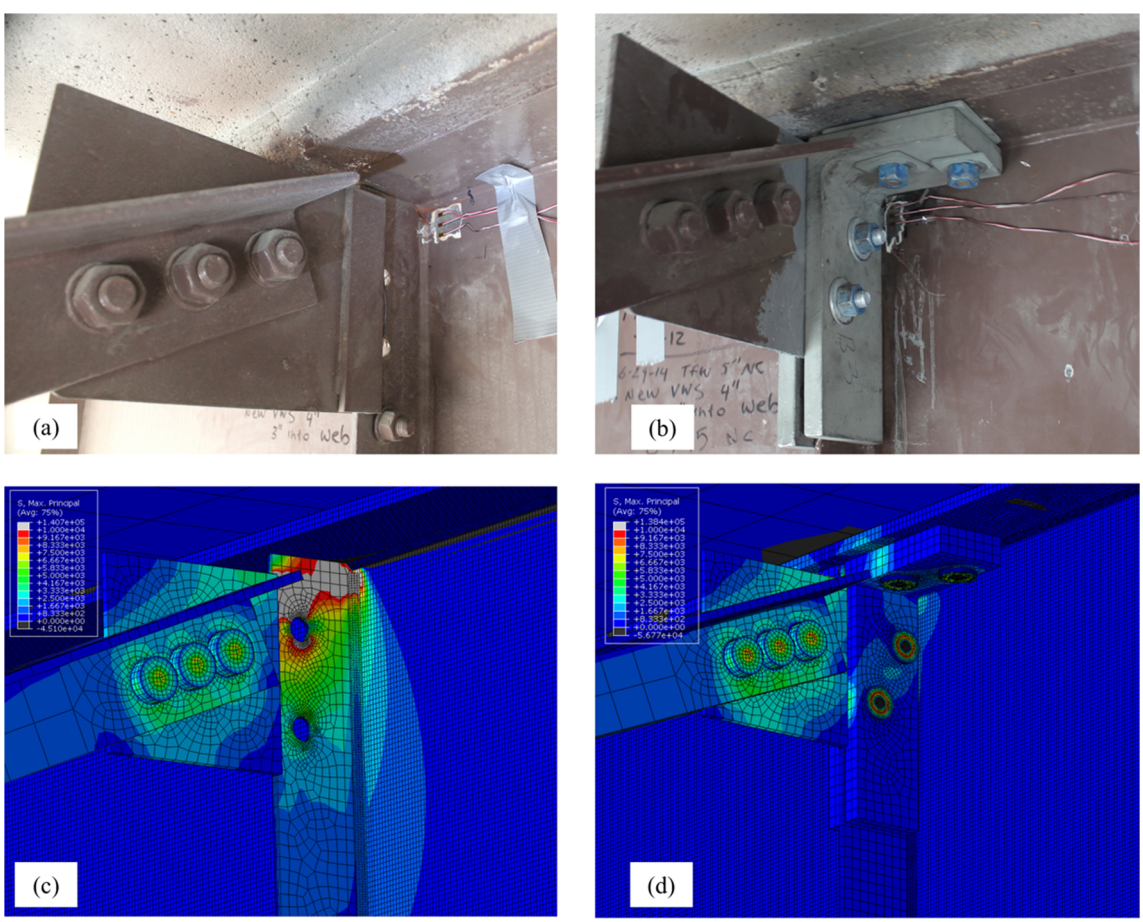

Fig. 18. Web-Gap instrumentations for the (a) first field test, (b) second field test, stress distribution obtained from FE for the (c) model before repair, and (d) model after repair.

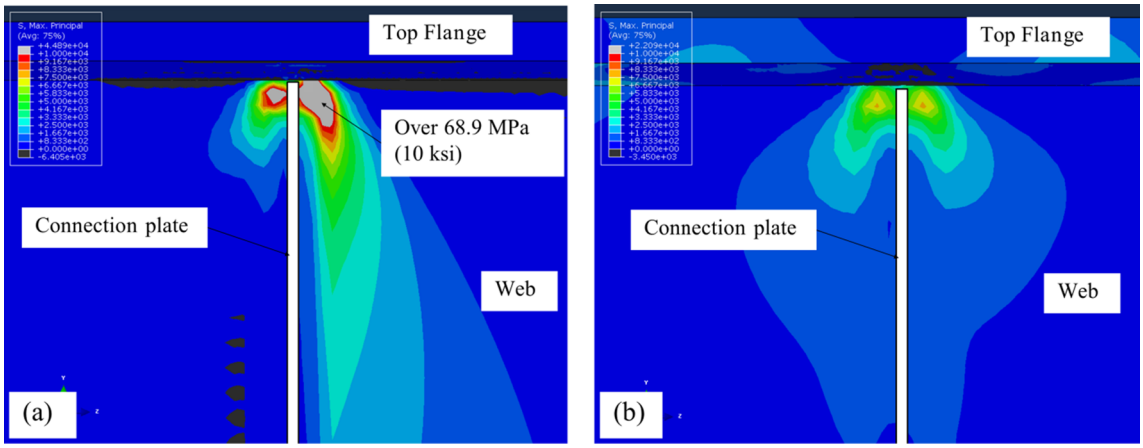

Fig. 19. Maximum principal stress contours in the web-gap region of G2 for the (a) before repair and, (b) after repair.

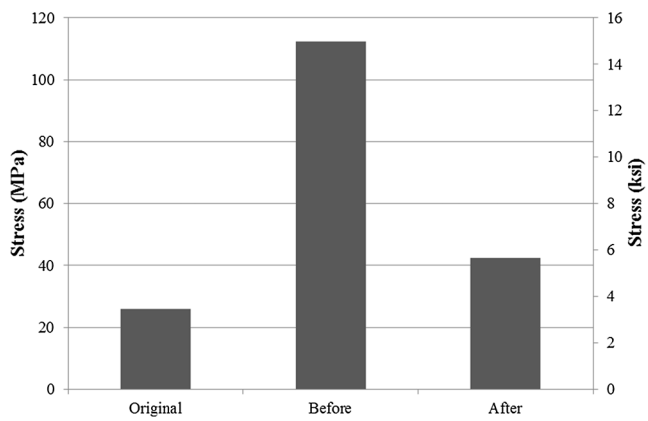

Fig. 20. Web-gap stress comparison at G2 before and after repair from the FEA.

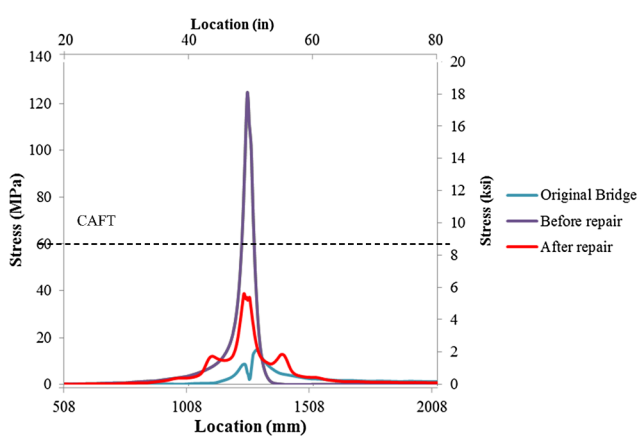

Fig. 21. Comparison between maximum principal stresses along the horizontal fillet weld of the web-to-flange joint before and after repair.

(G2 and G4) compared to the first field test conducted prior to installation of the repair angles.

- The stress in the web-gap region of G2 was reduced by 92% following the repair when the middle lane was loaded. The reduction was 91% and 21% when the truck was located in the right and left lanes, respectively.
- The stress in the web-gap region of G4 was reduced by 74% following the repair when the middle lane was loaded. The reduction was 93% and 81% when the truck was located in the right and left lanes, respectively.
- Based on the FE analysis, the maximum localized stress after the repair occurred at the same location before the repair, indicating the new load path through the repair angle section did not introduce a new critical fatigue sensitive area.
- A comparison between the FE results before and after the repair indicate that the repair is able to reduce the hot-spot stress and the peak stress along the horizontal fillet weld of the web-to-flange to about half of the CAFT. Consequently, the number of cycles leading to distortion-induced fatigue cracks can be increased.
- The study underlined the great importance of FE application in structural investigations before conducting a seismic retrofit for the bridges built before 1980s. Considering the FE proved implementing the top-angle retrofit/repair method significantly reduced the stress, the fatigue crack initiation and growth could be prevented by a preliminary FE study.

Acknowledgments

Support for the research described in this paper was provided by the Missouri Department of Transportation under project number TR201602. The authors highly appreciate the kind cooperation and assistance of Mark Croarkin, the former district bridge engineer, Joseph J. Molinaro, and Zachary G. Evans. The authors also thank Daniel Tobias from the Illinois Department of Transportation and Dr. Ying T. Chen for their assistance throughout the preparation of this manuscript. Also, special thanks go to Darren Green, engineering technician at Civil Engineering Department, Nick Duong, and Li Hui research assistants at SLU.

References

[1] Zayati F, Mahin SA. Evaluation of a seismic retrofit concept for double-deck reinforced concrete viaducts; 1996.
[2] Finke J. Construction of seismic retrofit strategies of the US 40/I-64 double deck bridge complex; 2006.
[3] Yen WP, O'Fallon JD, Cooper JD, Ger JJ. FHWA bridge seismic retrofit manual and its applications in Missouri Highway Bridges. Structures 2001@ sA structural engineering odyssey. ASCE; 2001. p. 1–8.
[4] Buckle I, Friedland I, Mander J, Martin G, Nutt R, Power M. Seismic retrofitting manual for highway structures: part 1-bridges; 2006.
[5] Jajich D, Schultz AE. Measurement and analysis of distortion-induced fatigue in multigirder steel bridges. J Bridge Eng 2003;8:84–91.
[6] Khalil A, Wipf TJ, Greimann L, Wood DL, Brakke B. Retrofit solution for out-of-plane distortion of X-type diaphragm bridges. Transportation conference proceedings. Iowa Department of Transportation; 1998. p. 99–102.
[7] Keating P, Saindon K, Wilson S. Cross frame diaphragm fatigue and load distribution behavior in steel highway bridges; 1997.
[8] Albuquerque C, Silva AL, de Jesus AM, Calçada R. An efficient methodology for fatigue damage assessment of bridge details using modal superposition of stress intensity factors. Int J Fatigue 2015;81:61–77.
[9] Alencar G, Jesus AMd, Calçada RA, Silva JGSD. Fatigue life evaluation of a composite steel-concrete roadway bridge through the hot-spot stress method considering progressive pavement deterioration. Eng Struct 2018;166:46–61.

[10] Horas CS, Correia JA, De Jesus AM, Kripakaran P, Calçada R. Application of the modal superposition technique combined with analytical elastoplastic approaches to assess the fatigue crack initiation on structural components. Eng Fract Mech 2017;185:271–83.
[11] Faraz S, Helmi K, Algohi B, Bakht B, Mufti A. Sources of errors in fatigue assessment of steel bridges using BWIM. J Civ Struct Health Monit 2017;7:291–302.
[12] Cai S, Chen W, Kashani MM, Vardanega PJ, Taylor CA. Fatigue life assessment of large scale T-jointed steel truss bridge components. J Constr Steel Res 2017;133:499–509.
[13] Kong X, Li J, Collins W, Bennett C, Jo H, Jeong J-H, et al. Dense capacitive sensor array for monitoring distortion-induced fatigue cracks in steel bridges. Sensors and smart structures technologies for civil, mechanical, and aerospace systems 2018. International Society for Optics and Photonics; 2018. p. 105980Q.
[14] Keating PB, Wilson SD, Kohutek TL. Evaluation of repair procedures for web gap fatigue damage; 1996.
[15] Hu Y, Shield CK, Dexter R. Use of adhesives to retrofit out-of-plane distortion induced fatigue cracks; 2006.
[16] Dexter RJ, Ocel JM. Manual for repair and retrofit of fatigue cracks in steel bridges; 2013.
[17] Hartman A, Bennett C, Matamoros A, Rolfe S. Innovative retrofit technique for distortion-induced fatigue cracks in steel girder web gaps. Bridge Struct 2013;9:57–71.
[18] Bun SH, Bonet E, Matamoros A, Bennett C, Barrett-Gonzalez R, Li J, et al. Improving infrastructure sustainability 2: repairing existing fatigue cracks in steel bridges using carbon fiber reinforced polymer materials; 2016.
[19] Fisher JW. Distortion-induced fatigue cracking in steel bridges. illustrated ed. Transportation Research Board, National Research Council; 1990.
[20] Stallings J, Cousins T, Stafford T. Removal of diaphragms from three-span steel girder bridge. J Bridge Eng 1999;4:63–70.
[21] Keating P, Crozier A. Evaluation and repair of fatigue damage to midland county bridges. Final report; 1992.
[22] Liu H, Zhou J, Bun S, Simmons G, Bennett C, Matamoros A, et al. Effectiveness of crack-arrest holes under distortion-induced fatigue loading. J Bridge Eng 2017;23:04017141.
[23] Connor RJ, Fisher JW. Identifying effective and ineffective retrofits for distortion fatigue cracking in steel bridges using field instrumentation. J Bridge Eng 2006;11:745–52.
[24] Shifferaw Y, Fanous FS. Field testing and finite element analysis of steel bridge retrofits for distortion-induced fatigue. Eng Struct 2013;49:385–95.
[25] Motaleb M, Duong N, Lindquist W, Hindi R. Investigation of distortion-induced web-gap cracking in a seismically retrofitted steel bridge: repair measures. J Bridge Eng 2016:04016139.
[26] Lindquist W, Ibrahim A, Tung Y, Motaleb M, Tobias D, Hindi R. Distortion-induced fatigue cracking in a seismically retrofitted steel bridge. J Perform Constr Facil 2015;30:04015068.
[27] MoDOT. St. Louis district traffic volume and commercial vehicle count map. Missouri Department of Transportation; 2013.
[28] Banan M, Capron MR. Seismic retrofit of the US-40/I-64 double-deck approach to poplar street bridge in St. Louis. Structures 2001@ sA structural engineering odyssey. ASCE; 2001. p. 1–7.
[29] MANUAL I. 4WFBS120, 4WFBS350, 4WFBS1K 4-wire full-bridge terminal input modules (TIMs). Campbell Scientific; 2017.
[30] ABAQUS. ABAQUS 6.14 analysis user's manual. USA; 2014.
[31] Fisher JW, Barthelemy B, Mertz D, Edinger J. Fatigue behavior of full-scale welded bridge attachments. Bethlehem (PA): Final Report Lehigh Univ; 1980. p. 1.
[32] AASHTO. LRFD bridge design specifications. Washington, DC; 2012.